Abschlussbericht zum Forschungsstipendium der Max-Buchner-Forschungsstiftung mit der Kennziffer MBFSt 2902

Analyse der Tropfeninteraktion zur Modellierung von Koaleszenzprozessen in Flüssig/Flüssig Dispersionen

Analysis and modeling of droplet-droplet interaction and particle-droplet interaction in dispersions

Stipendiat: M.Sc. Xinggang Li
Betreuer: Prof. Dr.-Ing. habil. Udo Fritsching
Particles and Process Engineering Department, Bremen University
Badgasteiner Str. 3, D-28359 Bremen, Germany

Abstract

Droplet (fluid) -droplet (fluid) interaction: A numerical investigation of binary droplet collisions in a gaseous phase has been conducted as part of the coalescence modeling project. A volume of fluid (VOF) based interface capturing method, which is characterized by introducing an extra artificial compression term into the volume-fraction transport equation, is employed to capture the liquid-gas interface. The full Navier-Stokes equations coupled with the volume-fraction transport equation are discretized on a fixed, uniform grid using the finite volume method. The solution of the volume-fraction transport equation is bounded by an explicit universal multi-dimensional limiter. The simulations cover the coalescence regime of binary droplet collisions. A ghost cell method is introduced in order to simulate retarded coalescence in head-on collisions. In this method, the volume-fraction boundary condition on the symmetry plane is switched to numerically control coalescence at a critical time which is determined by tracking the interface front. The simulated results are compared with attainable experimental data and provide detailed pictures exhibiting the collision processes. The inter-droplet pressure, defined by the static pressure on the symmetry plane in head-on collisions, is evaluated. The phenomenological criteria for droplet coalescence model are discussed. Moreover, the multiple entity VOF model and adaptive local grid refinement approach are implemented in OpenFOAM and tested here. For the former, by using two or more VOF indicator functions, the identity of each droplet is preserved and can be detected after contact until coalescence. The multiple entity VOF model is helpful to develop the droplet coalescence model here. For the latter, it can be combined with VOF model to increase the accuracy of the solution particularly in the region of the liquid-gas interface and thus has a potential to capture more details of tiny satellite droplets' formation.

Particle (solid) -droplet (fluid) interaction: Particle-droplet interaction is modeled by VOF method coupled with mesh motion in six degrees of freedom (6-DoF). Here the small solid particle (in the order of 1~10 μm) is represented by a solid object with 6-DoF motion while the liquid droplet (in the order of 10^2 μm) represented by liquid volume fraction. The preliminary results are presented in this report.

Part I: Modeling of droplet-droplet interaction

Compressive VOF: In this report, the focus is on the collision process of two equal-sized droplets in a gaseous atmosphere at moderate Weber numbers. Qian and Law [1] presented well time-resolved photographic collision images in all collision regimes for a hydrocarbon/nitrogen system, which have been used as validation reference here. The numerical simulation is performed using the open source CFD code OpenFOAM [2]. A VOF based interface capturing method is applied to deal with the gas-liquid interface. In OpenFOAM, the necessary compression of the interface is achieved by introducing an extra, artificial compression term into the volume-fraction transport equation instead of just using a compressive differencing scheme. Multi-dimensional universal limiter with explicit solution (MULES) (i.e., the current approach to define the compressive velocity field in OpenFOAM) is used to limit the flux of the variables to guarantee a bounded-solution. The continuum surface force (CSF) method is employed to calculate the surface tension force. However, as in the standard VOF

method, an immediate coalescence happens automatically whenever two interfaces enter one grid cell. In order to overcome this problem, some tricks are applied, e.g., the ghost cell method in Jiang and James [3] or using two VOF indicator functions in Nikolopoulos et al. [4].

Ghost cell method: Head-on collisions of two equal-sized droplets are identical to the collision of one droplet with symmetry plane, which is perpendicular to the colliding direction. The droplet in the computational domain will interact with its mirror image through the volume-fraction boundary condition on the symmetry plane. Different volume-fraction boundary conditions will lead to different collision outcomes. For example, on the symmetry plane, with symmetry conditions for other variables such as velocity and pressure, zero condition for liquid volume fraction will lead to bouncing while symmetry condition to coalescence. In the finite volume method, the volume-fraction boundary conditions are set in the ghost cells just outside the physical boundaries, i.e., the symmetry plane here. The volume fraction is zero in each ghost cell if a zero boundary condition is applied, and is equal to the value in the adjacent real cell if the symmetry boundary condition is applied. The layer of ghost cells with a zero volume fraction can be regarded as a perfect gas layer, and thus always leads to bouncing at last. Assuming a retarded coalescence collision firstly experiences a similar process as bouncing and then is followed by an immediate coalescence before the droplets depart from each other, the simulation of retarded coalescence during head-on collisions can be divided into two stages based on the above assumption: 1) computing with a zero volume-fraction boundary condition on the symmetry plane to simulate a pre-bouncing process; 2) switching to a symmetry boundary condition to simulate a post-coalescence process. The critical time to switch boundary conditions is defined when the thickness of the inter-droplet gas film achieves a minimum value. At the critical time, the droplets don't have enough kinetic energy to squeeze the gas film further and will determine whether to coalesce or bounce. Therefore, this critical time can also be designated as the gas film rupture time for coalescence or the rebound time for bouncing. If the boundary condition of the volume fraction is switched into symmetry condition at this moment, which means the complete rupture of the inter-droplet gas layer, allowing coalescence to occur. Otherwise, the gas layer is kept and the droplets will bounce apart.

Two VOF indicator functions: A separate VOF variable is assigned to each droplet, i.e., 'α_1' for the first droplet and 'α_2' for the second. Consequently each droplet is separately tagged thus eliminating the merging of the two droplets at impact.

It should be mentioned that, as the inter-droplet gas film or double interface between two droplets are removed in above methods, there is a reduction in surface energy due to the elimination of the common surface between the droplets; but in reality this energy is supposed to be dissipated when the ruptured film breaks into small droplets or to be stored as surface energy of these small droplets. The kinetic energy is not altered by the rupture.

Adaptive local grid refinement approach: The mesh adaptation category of *h*-refinement is implemented, where computational points are inserted inside the computational domain [5,6]. The criterion for the mesh refinement is the solution accuracy and/or the gradient of liquid volume fraction (α). To account for the high flow gradients near the free surface interface, the cells are subdivided into a number of resolution levels in either sides of the free surface. As a result, the interface always lies in the densest grid region (as shown in Fig. 1). When a new grid with 1 level of local refinement is created an initial cell is split into eight secondary cells (for three dimensional problems).

Numerical solution procedure: The governing equations are solved numerically using a finite volume method on a fixed, uniform Cartesian mesh. As in Pan and Suga [7], for all the cases, the droplet diameter D_0 is resolved by at least 60 cells, e.g., D_0/Δ = 60-100, where Δ is the cell size. The time derivative is discretized using the Euler scheme. The discretization of the divergence terms is based on the TVD schemes, e.g., the VanLeer scheme for the divergence term of the volume-fraction and the limited linear differencing scheme for the divergence term of the velocity. For the artificial compression term, the so called 'interfaceCompression' scheme is implemented in OpenFOAM [8]. The laplacian terms are discretized using the central difference scheme. The correctors to the momentum equation and the vol-

ume-fraction convection equation are calculated through the PISO or PIMPLE loop. The time step is adjustable automatically to keep Co number below the specified maximum value (preferred 0.2).

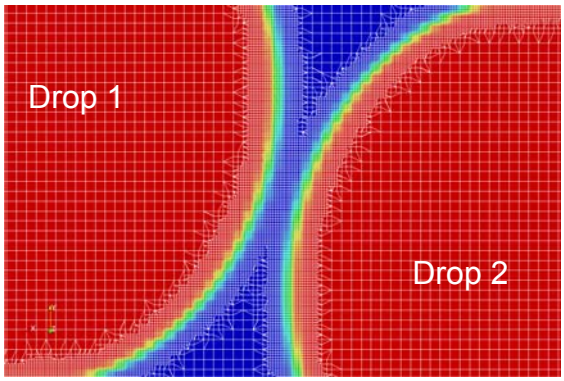

Figure 1: New mesh around interface after two level of local refinement

Numerical results from compressive VOF + ghost cell method

Variation of inter-droplet distance: In order to simulate retarded coalescence, one key issue is to determine the rupture time of the inter-droplet gas film, which is defined when the minimum thickness of the gas film is achieved. The minimum cell size used in the simulation is around 3.3 μm and is too large to capture a real gas film in the order of 10^2 Å. However, the movement of the interface front, which is located by the isosurface of f = 0.5, can be tracked and the real gas film thickness can be qualitatively represented by the inter-droplet distance Δh. Firstly, cases A~D are computed with a zero volume-fraction boundary condition on the symmetry plane. The contours of two droplets can be obtained by mirroring the results around the symmetry plane. The data of Δh are measured at different positions of the flatten region and averaged. The function of the inter-droplet distance Δh vs. time is shown in Fig. 2. The starting time t = 0 is defined at the moment when the two droplets contact with each other according to the initial impact velocity. After the first stages of the collision, the interface moves very slowly, but the receding of the interface front can be detected. For cases A~D, the gas film rupture times or the rebound times are approximately at t = 0.75 ms, 0.70 ms, 0.475 ms and 0.45 ms, respectively and the minimum inter-droplet distance is between 3-5 μm. The slight non-synchronization in the movement of the interface front can be found in cases A and B at some moments, which means the gas layer between the droplets is not always flat or smoothing. It seems the case with a higher Weber number possesses a thinner gas layer and a shorter rupture time of the inter-droplet gas film, indicating that coalescence happens more easily for such cases. But coalescence also happens at lower Weber numbers as in regime I. Qian and Law [1] speculated that the tendency of the final merging of the droplets' surface in this regime may be controlled by the intermolecular force.

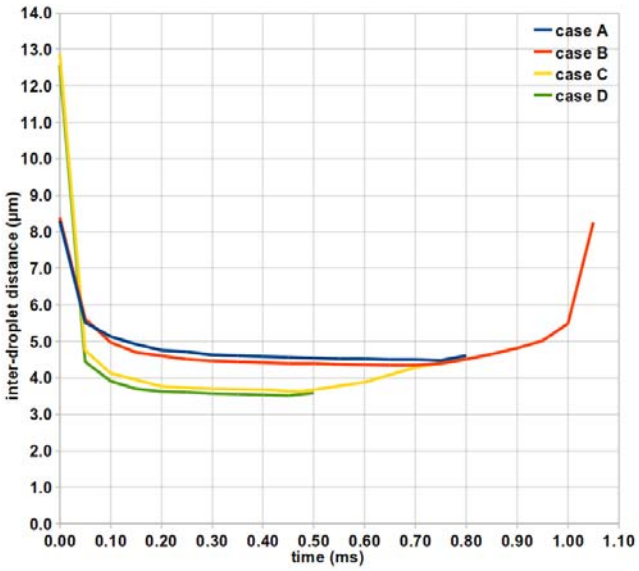

Figure 2: Inter-droplet distance with time for cases A~D, A: (*We, Re, I, D_0*) = (0.2, 14.8, 0, 240μm); B: (*We, Re, I, D_0*) = (0.5, 23.6, 0, 262μm); C: (*We, Re, I, D_0*) = (8.6, 105.9, 0, 306μm); D: (*We, Re, I, D_0*) = (15.2, 139.8, 0, 302μm)

Retarded coalescence with minor deformation: In case A, the droplets experience a small deformation and then coalesce permanently. In the simulation, case A is regarded as a retarded coalescence case. Firstly, a zero volume-fraction boundary condition is applied on the symmetry plane; at the critical time, it is then replaced by the symmetry condition. A sequence of time-resolved images is generated from the simulation for a direct comparison with the experimental results. As exhibited in Fig. 3(b), the droplets impact with each other at t = 0.65 ms and the gas film ruptures at t = 1.40 ms. After reaching a maximum deformation around t = 1.20 ms, the droplets start to move away from each other and then a stretched liquid cylinder is formed at t = 1.70 ms. At last, the cylinder is pulled into a sphere by surface tension. Most of features as in the experiment can be captured, but the droplet evolution advances faster in the simulation, especially after coalescence of droplets. The discrepancy may be mainly caused by the slightly different impact numbers.

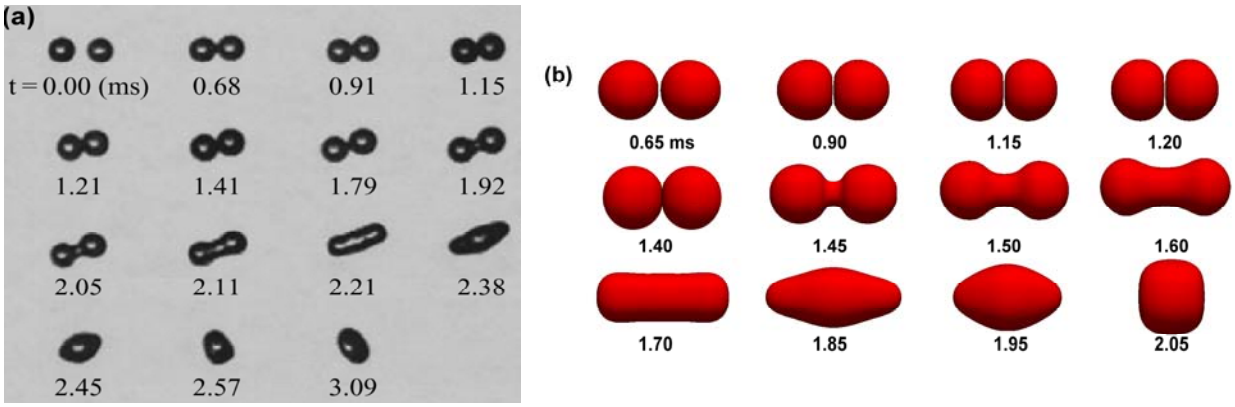

Figure 3: Case A -Retarded coalescence with minor deformation; (a) Experiment of Qian and Law [1], (*We, Re, l, D_0*) = (0.2, 14.8, 0.20, 240μm); (b) Simulation (*We, Re, l, D_0*) = (0.2, 14.8, 0, 240μm)

Retarded coalescence with major deformation: In case D, the two colliding droplets will also experience a retarded coalescence at higher We-number. Therefore, at the beginning, a zero volume-fraction boundary condition is applied on the symmetry plane. The rupture of the gas film occurs at t = 0.55. Due to the high initial kinetic energy, the droplets experience a substantial deformation compared with case A. It can be seen that the simulation results at various time instants agree with the experimental results very well. Around t = 0.40 ms, the maximum deformation is achieved in both simulation and experiment. The rupture time of the gas film is also well predicted, e.g., it can be observed that at t = 0.54 ms in Fig. 4(a), the cusp at the rim of the inter-droplet gap disappears and a round profile is built, indicating coalescence happens; at t = 0.55 ms in Fig. 4(b), the gas layer between the droplets is removed and the droplets start to coalesce. Only the rotation action is not captured by simulation due to the slight difference in impact numbers (0.08 in experiment vs. 0 in simulation).

Inter-droplet pressure: The inter-droplet pressure is defined by the static pressure on the symmetry plane. Fig. 5 and Fig. 6 show the inter-droplet pressure as a function of time and radial position. The starting time is defined when the droplet contacts with each other. For cases A and D, only the pressure variations before the rupture of the gas film are presented. For all the cases, at the first stages, there is a dramatic increase in the pressure as the droplets approach each other and then a high pressure region between them forms and expands radially outward until a maximum contact area is achieved. Case A experiences minor deformations and only narrow regions of high pressure form between the droplets. The pressure changes between the droplets are not smooth and some disturbance can be observed. This phenomenon implies the mechanism of the rupture of inter-droplet gas film at low Weber numbers may be related to point-rupture. Case D experiences large deformations due to their higher Weber numbers and broad regions of high pressure can be built between the

droplets. The pressure in these regions varies smoothly in the radial direction and no disturbance is observed, which implies the mechanism of the rupture of inter-droplet gas film may be related to plane-rupture at high Weber numbers.

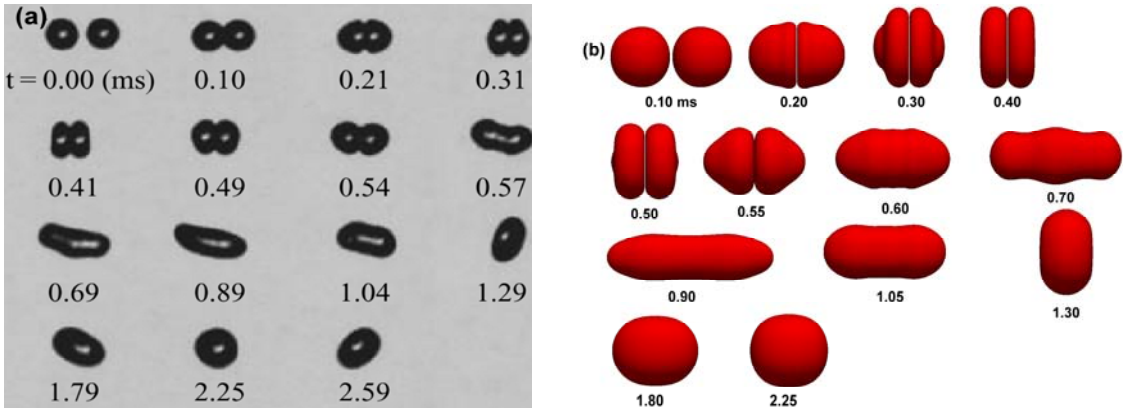

Figure 4: Case D - Retarded coalescence with major deformation; (a) Experiment of Qian and Law [1]), (*We, Re, I, D_0*) = (15.2, 139.8, 0.08, 302μm); (b) Simulation (*We, Re, I, D_0*) = (15.2, 139.8, 0, 302μm)

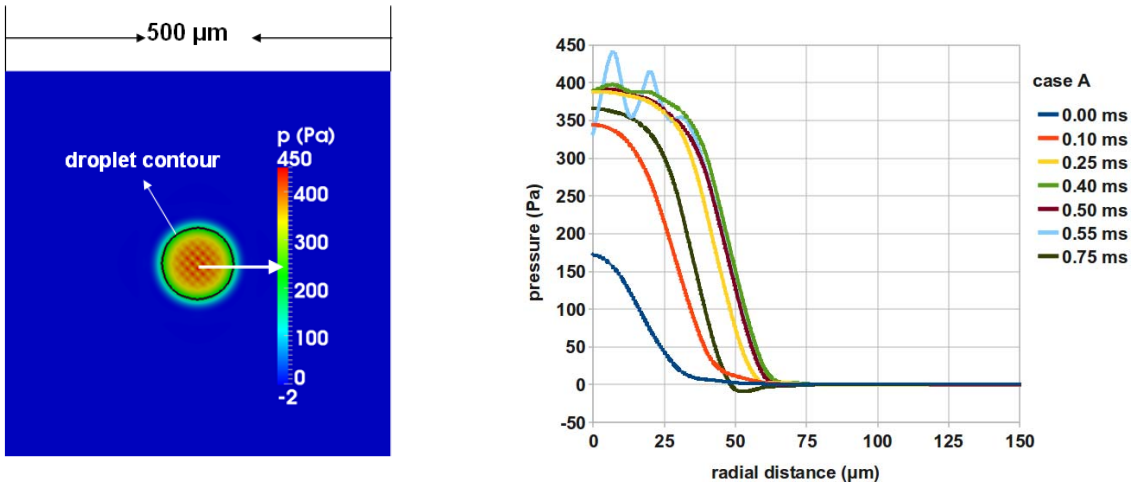

Figure 5: Pressure field on the symmetry plane (left) and inter-droplet pressure as a function of time and radial position for cases A

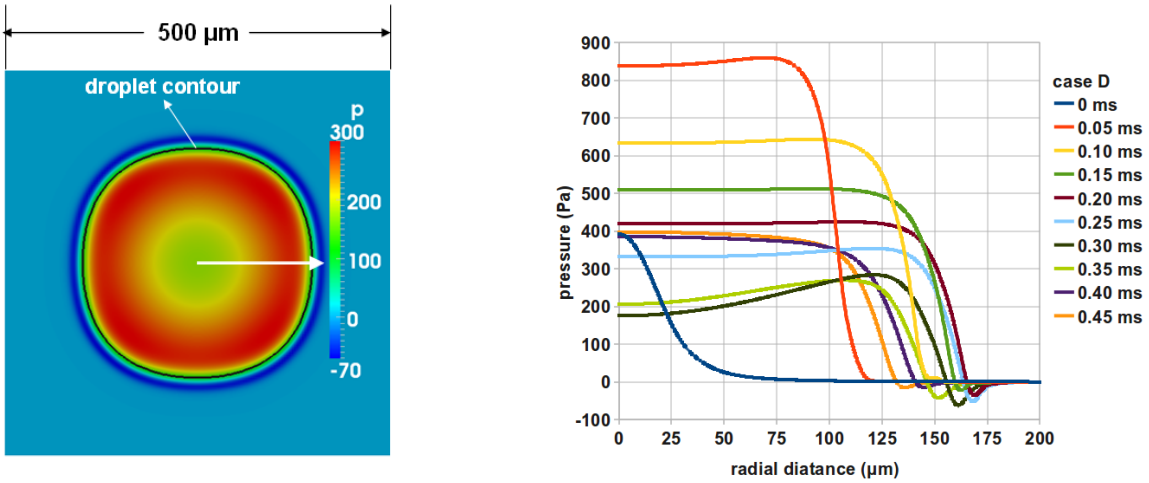

Figure 6: Pressure field on the symmetry plane (left) and inter-droplet pressure as a function of time and radial position for cases D

The pressure values in the high pressure regions are collected and averaged at every moment for cases A~D. A pressure coefficient C_p is introduced, which is defined by the ratio of the inter-droplet pressure and the initial droplet kinetic energy, in the form $C_p = 2p/(\rho_{liq} * U_0\text{^}2)$. A higher value of C_p means a larger barrier for droplets to coalesce. The function of C_p vs. time is plotted for cases A~D in Fig. 7. It can be observed the value of C_p decreases with increasing Weber numbers, and that means the droplets with higher Weber numbers can overcome the pressure barrier to coalesce more easily than those with lower Weber numbers. The exception is still in regime I, where the droplets possess very small Weber numbers but coalesce permanently, possibly due to the strong influence of molecular forces which is not considered in the macroscopic CFD governing equations. From the *We-I* diagram [1], cases B and C are located in bouncing regime. As shown in Fig. 7, it can be observed that, C_p variation in the retarded coalescence cases performs similarly before coalescence as that in the bouncing cases with close Weber numbers and impact numbers.

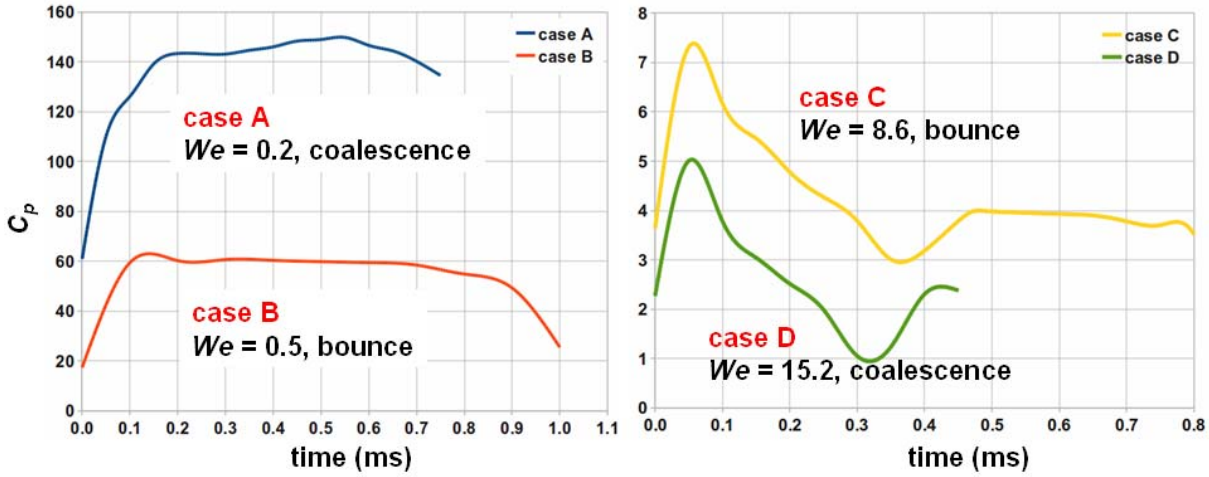

Figure 7: Comparison of the ratio of the inter-droplet pressure and the initial droplet kinetic energy with time for cases A~D

The variation in the inter-droplet pressure depends on the movement of the interface front and the drainage rate of the inter-droplet gas film. The forward movement of the interface front will squeeze the inter-droplet space to increase the inter-droplet pressure while the passive drainage of the gas film will reduce the pressure. Case C is taken as an example to analyze the changes of inter-droplet pressure with time by combining a qualitative analysis of velocity field evolution. Fig. 8 exhibits the velocity field evolutions of case C and the isosurface of f = 0.5 is shown to indicate the position of the droplet. At t = 0.00 ms, a sheet jet and vortex ring are built. Because of the strong initial kinetic energy, a high pressure peak is achieved in a short time, but the forward velocity of the interface front is also reduced greatly while the drainage of the gas film turns stronger (Fig. 8, t = 0.10 ms). From t = 0.05 ms, due to the large deformation, the drainage of the gas film plays a main role and the inter-droplet pressure decreases until a maximum deformation is achieved at t = 0.35 ms. As depicted in Fig.8, at the moment of t = 0.40 ms, the vortex has already changed the rotational direction and also weakened the drainage of the gas film greatly. Therefore, the inter-droplet pressure increases again. At t = 0.50 ms in Fig. 8, it can be observed that the reverse vortex becomes stronger and nearly the whole droplet is reversed. The interface front starts receding and the droplet pressure decrease again.

Numerical results from compressive VOF model

Immediate coalescence: Depending on whether the retardation time is negligible or not, coalescence regime can be divided into two parts: retarded coalescence collisions in the region of low Weber numbers and immediate coalescence collisions in the region of high Weber numbers. Case E is in the latter part, where the droplets almost merge immediately once they contact with each other. For immediate coalescence collisions, there is no need to employ the ghost cell method to retard the coalescence due to a negligible rupture time of the

inter-droplet gas film. Fig. 9 shows the comparison between the experiment and the simulation results. Again, a reasonable agreement is obtained. Unlike case D, the two droplets coalesce at once after their contact. At t = 0.25 ms, a maximum deformation is reached, forming a boundary ring with a thin connecting liquid disk inside. Subsequently, the radial velocity reverses its direction towards the centre of the disk, and the ring shape is gradually transformed into a dumb-bell shape (Fig. 9, t = 1.80 ms) due to an outwardly directed axial internal flow. However, this outward motion is not sufficient to separate the coalesced droplets and finally the end of the bell is pulled back by the surface tension, forming a spherical droplet. It should be pointed out that the images between t = 1.20 and 2.00 ms show a thicker neck between the knobs compared with the experiment, which may be related to the drawback of CSF method: a modeled surface tension force acting on an interface of finite thickness will bring some discrepancies particularly in low Weber number regimes if the mesh is not refined enough.

For the cases in reflexive separation and stretching separation regimes, the binary droplets will coalesce immediately due to the large initial kinetic energy once they touch each other, followed by mass deformation and separation sometimes as well as satellite droplets' formation. The compressive VOF model can be directly employed. The simulation results of reflexive separation and stretching separation were compared with experimental results in Li and Fritsching [9] and an acceptable agreement is obtained. In this report, adaptive mesh refinement technique is coupled into VOF method in order to capture more details of satellite droplets' formation. In Fig. 10, the comparison is made between experimental results and simulation results from VOF model (Mesh: ~10 million cells; Execution time: 2 months) and VOF model coupled with adaptive mesh refinement technique (Base mesh: 0.5 million cells; Final mesh with two levels of refinement: 5 million; Execution time: three weeks). With two levels of refinement, the combination of VOF model and adaptive mesh refinement technique shows similar accuracy but higher efficiency compared with VOF model. Higher refinement levels may bring more accurate results but higher computational cost.

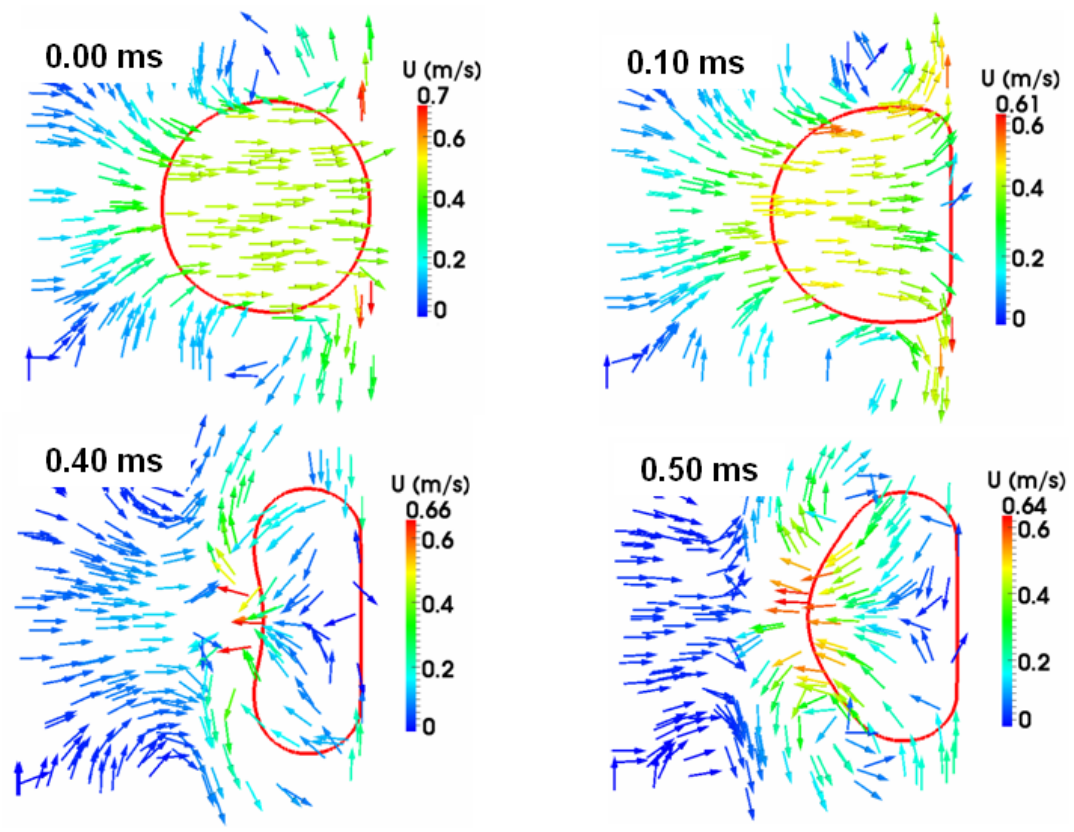

Figure 8. Velocity field evolution for case C

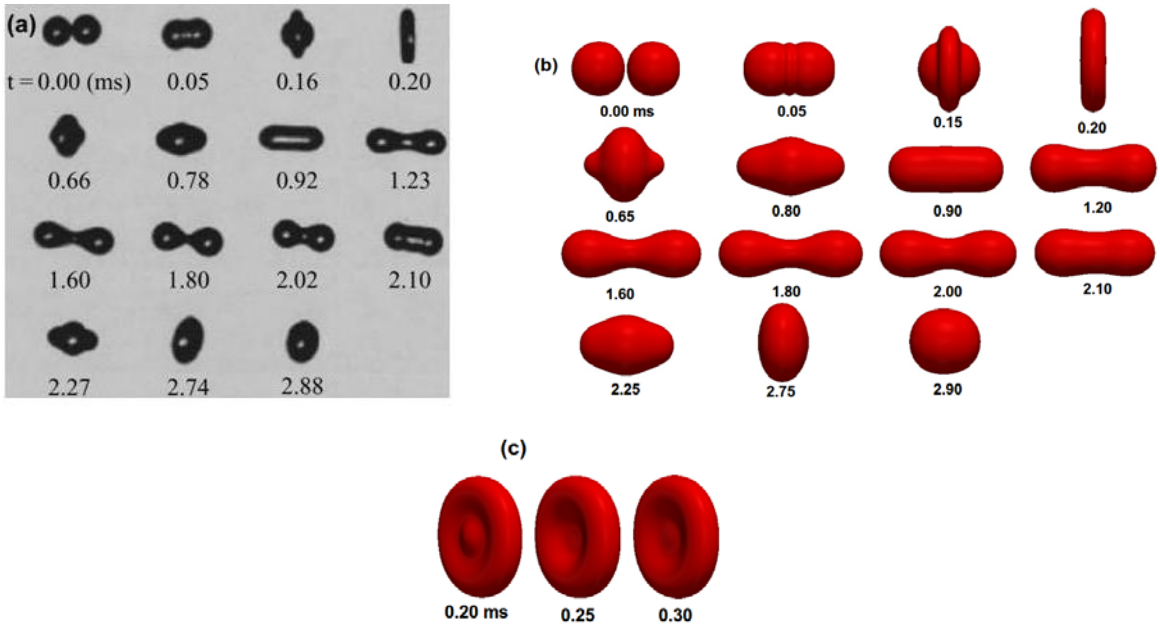

Figure 9: Immediate coalescence with major deformation (a) Experiment of Qian and Law [1], (*We, Re, I, D_0*) = (32.8, 210.8, 0.08, 318μm); (b) Simulation of case E, (*We, Re, I, D_0*) = (32.8, 210.8, 0, 318μm); (c) Perspective view angle

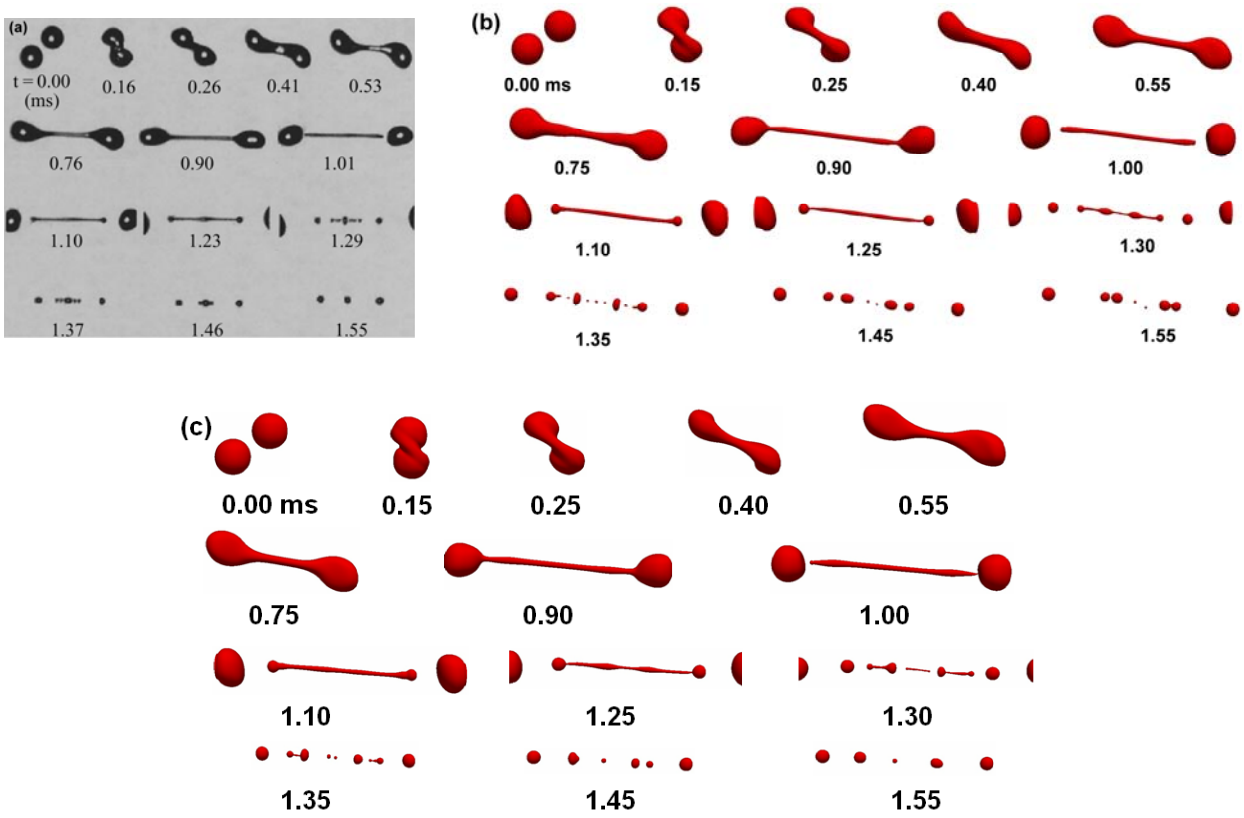

Figure 10: Stretching Reflexive separation with satellite droplets (a) Experiment of Qian and Law [1], (*We, Re, I, D_0*) = (64.9, 312.8, 0.71, 354μm); (b) VOF model; (c) VOF model + adaptive local grid refinement approach

Numerical results from two-VOF-indicator model

If a single VOF variable is used then, upon contact, the two droplets will immediately coalesce, which is not correct for low Weber number impact. In order to overcome this problem, a separate VOF variable is assigned to each droplet, i.e., 'α_1' for the first droplet and 'α_2' for the second. Consequently each droplet is separately tagged thus eliminating the merging of the two droplets at impact. This method is used to model the coalescence retardation procedure, and then the double interfaces between the two droplets are simply removed at a prescribed time, leading to coalescence. In the present investigation, the prescribed coalescence time is determined by experiment. Take case D as an example (Fig. 4(a)), the cusp at the rim of the droplets in the gap area disappears between t = 0.54 ms and t = 0.57 ms. Therefore, the critical time can be fixed at t = 0.55 ms. Fig. 11 exhibits the simulation results and an acceptable agreement is obtained compared with experimental results (Fig. 4(a)).

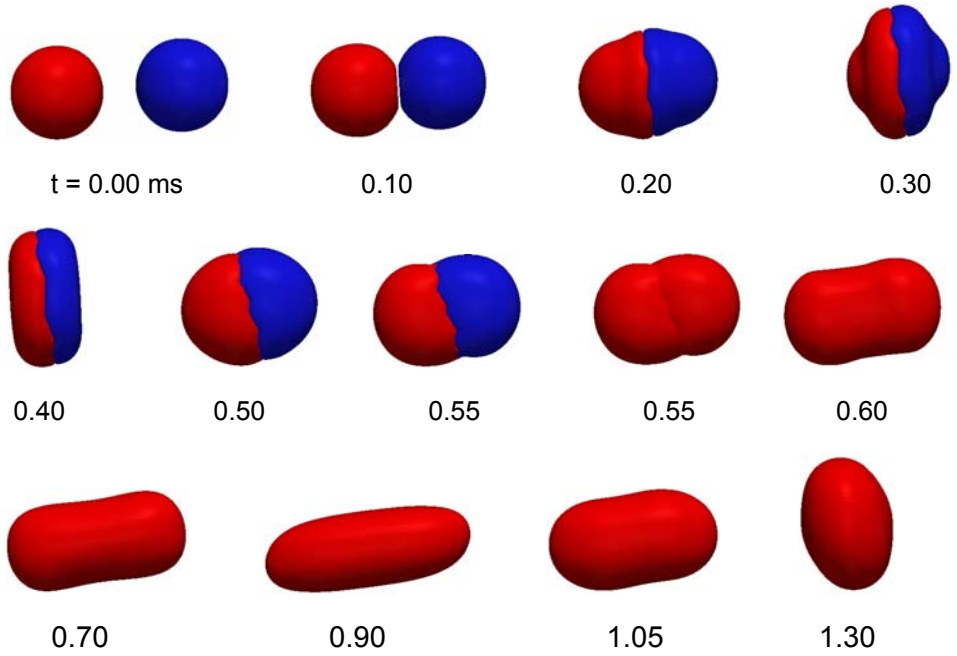

Figure 11: Retarded coalescence with major deformation: case D (We, Re, I, D_0) = (15.2, 139.8, 0.08, 302μm), simulation using two VOF indicator functions

Phenomenological criteria for droplet coalescence model

A CFD model is a common numerical strategy to predict liquid droplet collision process by means of Navier-Stokes (NS) equations (momentum and mass conservation) plus an interface capturing model, e.g., level set (LS) methods [7] and volume of fluid (VOF) [9] methods. In principle the direct outcome of a drop collision process needs to be described depending on micro-scale effects (that may occur on the sub-grid scale) in the contact zone as e.g. the local flow conditions in the inter-droplet film as well as physico-chemical interactions between the liquid surfaces. However, based on the understanding of the physical criterion that determines the outcome of the collision (coalescence or bouncing) some phenomenological conclusions can still be extracted from the description of macro-scale behavior of droplet contact by CFD models coupled with some 'tricks', e.g., the compressive VOF model plus ghost cell method in this report.

According to the physical criterion, coalescence may not occur readily when the droplets collide because of the presence of the gaseous film that needs to be drained out or broken up. Therefore, it's reasonable to build a gas layer before droplets' coalescence using ghost cell method. The resistance with which this inter-droplet film can be discharged then depends on the collision inertia of the droplets and the dynamics of the film flow including the pressure buildup within it. In this report, a non-dimensionless pressure C_p is introduced to describe this resistance. Conceptually, one would expect the complete release of the gas film is favored either for a sufficiently slow rate of approach (regime I: coalescence with minor deformation) such that there is enough time for discharge, or for a sufficiently high rate of approach (re-

gime III: coalescence with major deformation) such that the release is forcibly accomplished. Also, it is reasonable to expect that there should exist a regime II for moderate rates of approach, for which the discharge is not finished. In this case the colliding droplets lose all the impact inertia before merging due to the substantial pressure build up in the inter-droplet region as well as the conversion of part of the kinetic energy to surface energy through droplet deformation and the dissipation of the rest of it through viscous action. The deformed droplet mass subsequently bounces away and finally restores their spherical shape through surface tension. The above conception can explain why the coalescence can happen at both of high C_p (case A) and low C_p (case D) values. A higher C_p leads to a lower discharge rate and a longer discharge time (Li and Fritsching [9], see Fig. 12 and Fig. 13). Due to the long discharge time, it is appropriate to name regime I retarded coalescence with minor deformation. But due to the strong micro-scale effect, the macro-scale parameter C_p is not appropriate as a criterion in this regime. In Krause et al. [10], droplet contact time (not real contact), similar to the discharge time here, is used as a criterion for droplet coalescence at low Weber numbers (or regime I). In Krause et al. [10], contact of the phases in a cell is assumed when the product of the phase fraction gradients of different liquid entities is greater than zero and the contact time approach is initialized. A critical contact time is defined and above which the droplet volumes and interfaces will finally merge together. The contact area on the line of centers of the colliding droplets should be the 'oldest'. This critical contact time should depend on material and kinetic contact properties. In head-on collisions, the critical contact time may be determined by VOF-ghost cell method assuming the end time of the contact is defined when the gas film thickness achieves a minimum value. In regime III, the macro-scale behavior of the droplet contact plays a dominant role in droplet coalescence and the maximum non-dimensionless pressure $C_{p,max}$ can be used as a criterion. Coalescence happens if $C_{p,max}$ below a critical value while immediate coalescence if $C_{p,max}$ is negligible. For the case without regime II, e.g., water droplet collision in 1 atm air, both of critical contact time and critical maximum non-dimensionless pressure have a potential to be used as criteria for droplet coalescence.

Part II: Modeling of particle-droplet interaction

The present study aims to provide insight into physical interactions that take place when an injected ceramic particle collides with an atomized metallic droplet during spray atomization processing of particulate reinforced metal matrix composite (MMC) particles. During spray atomization, the molten alloy is energetically disintegrated into micrometer-sized droplets using high velocity jets of nitrogen gas inside an environmental chamber. Simultaneously, ceramic particles, conveyed by atomization gas or via a separate gas-assisted delivery system, are injected and impacted with metallic droplets. Possible interaction mechanisms between ceramic particles and metallic droplets may be divided into three categories. First, a particle may collide with a droplet and bounce back. Second, a particle may collide and attach to the surface of a droplet (surface rupture). Third, a particle may partially or completely penetrate a droplet and remain within the droplet. The particle/droplet collisions are desired to occur in the third category for the production of MMC particles.

The possible factors, influencing the penetration path of a particle, include a number of intensive properties (density, viscosity, surface tension and contact angle) and extensive properties like the ratio of droplet to particle size, impact velocity and impact direction. In the available literatures two approaches for modeling particle-droplet collisions have been found. The first approach is based on energy conservation [11, 12] while the other based on force balance [13]. In both approaches the collision partners are assumed to be spherical before impact and still spherical during the penetration. The particle moves with one degree of freedom and only head-on particle/droplet collisions were modeled. In the first approach, the driving force of the penetration is the initial kinetic energy of the particle. During the penetration the kinetic energy is used to overcome the change in surface energy. The kinetic energy is also dissipated due to the work done by the viscous drag acting on the particle. The model based on energy conservation has been used for modeling incorporation of ceramic particles into liquid metals [11, 12]. In the second approach, viscous drag force, surface tension force and capillary force are considered. The model based on force balance has been used to predict the outcomes of the collisions between recycled particles and atomized droplets in a spray drying process [13].

In this report, a CFD model is presented to numerically investigate the particle/droplet collision behavior. The CFD model describes the multiphase flow (gas/droplet/particle) by means of Navier-Stokes (NS) equations (momentum and mass conservation) plus VOF-6DOF method with mesh motion [14]. Here the small solid particle is represented by a solid object with 6 DOF motion while the liquid droplet represented by liquid volume fraction. The solid particle is moved by moving the points on the particle and the cells neighboring it. Moving points in a grid requires models and corresponding mesh motion equations to be solved. Here mesh motion model is based on mesh deformation method, where the cells in the mesh are deformed (stretched or squeezed) due to the motion of a part of the mesh (Fig. 12). A displacement Laplacian solver is selected, where the equations of cell motion are solved based on the Laplation of the diffusivity and the cell displacement. The diffusion algorithms described in [15] can be used. The mesh motion is described explicitly to the fields of the point displacement and cell displacement at each time step of the solver. A field of vectors is assigned to describe the accumulated displacement up to that time step. It should be mentioned that the mesh motion scheme here can be used in cases where the resolution is not changing too much during the mesh motion, i.e., relatively small changes in mesh occur, so that cell density changes do not affect the results during the computation. Therefore, for a fixed relative velocity between collision partners, both of particle and droplet are given initial velocities in order to reduce the displacement the particle moves. This also agrees with the facts that both of particle and droplet move in practice.

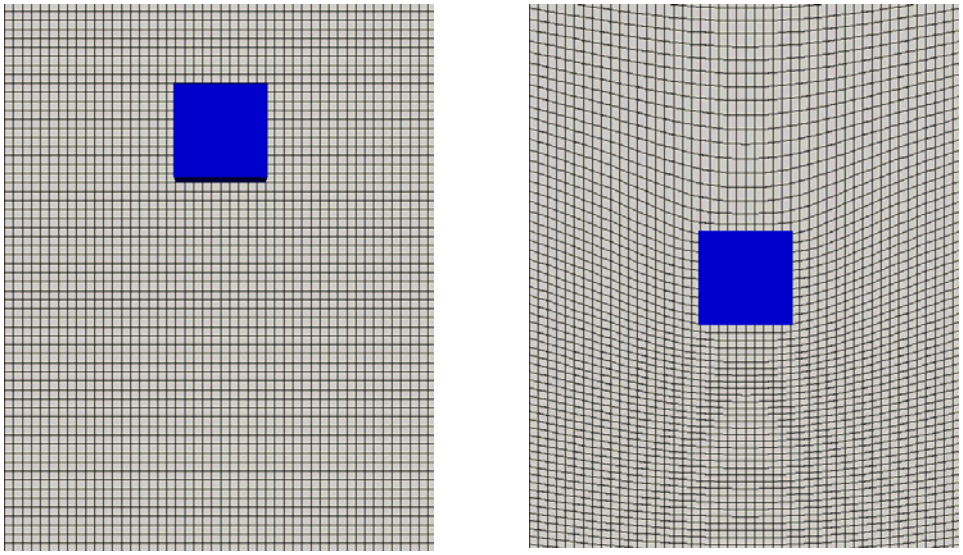

a) before particle move b) after particle move

Figure 12: Mesh deformation after mesh motion, cubic particle in blue

Compared with energy conservation and force balance approaches, the advantages of the CFD model are as follows: 1) Non head-on particle/droplet collisions can be easily modeled. 2) Setup of dynamic contact angle is available in VOF model, which is helpful to capture a more actual contact. 3) The deformation of liquid surface near the penetration area can be easily modeled by VOF model. As shown in Fig. 13, the droplet deformation can greatly store the kinetic energy (above 80%) before the particle rupture the droplet surface, slowing the particle down more than expected. 4) 3D simulation is available. The particle can move in six degrees of freedom and is not limited to only spherical shape. 5) Turbulence model can be easily coupled and thus the turbulent liquid flow near the penetration area at high Reynolds numbers (*Re*) can be modeled. 6) The viscous drag for the partially submerged particle in the droplet can be solved naturally by VOF model. 7) The forces considered in energy conservation and force balance approaches are taken into account implicitly in CFD model.

So far, no heat transfer model and liquid solidification model are implemented into the present CFD model. The fluids (gas / liquid metallic droplet) and solid (ceramic particle) are iso-

thermal. The physical properties of liquid tin (Sn) at temperature T = 550 K are used. In experiment the reinforcing ceramic particulates that are encountered in spray processed MMC particles, such as TiC, are generally of a size ranging from 1 to 25 µm, while the size of the final MMC particles ranges from 50 to 400 µm. The shape of the TiC particles is irregular while the final MMC particles are spheroidal. Therefore, a cubic particle of size 20 µm and a spherical droplet of size 120 µm are modeled. The static contact angle between TiC and liquid tin (Sn) is 84°.

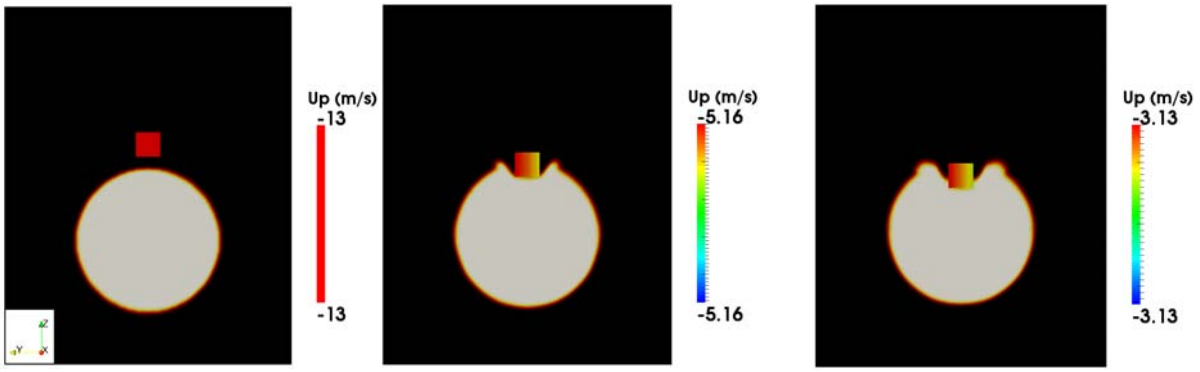

t = 0 ms t = 2 ms t = 4 ms

Figure 13: Cubic ceramic particle (TiC, a = 20 µm, $U_{p,0}$ = -13 m/s) penetrating into liquid metal droplet (represented by grey, tin (Sn), d = 120 µm, $U_{d,0}$ = 2 m/s), the color scale is only valid for cubic particle

The initial mesh consists of uniform hexahedral cells. The cubic particle is resolved by at least 10 cells. Mesh dependence tests have been performed using different mesh resolutions ranging up to the maximum and confirmed that the present results are reasonably mesh independent. As shown in Fig. 14, for the case with coarse mesh (Fig. 14 (a)), the calculation collapsed at t = 5 ms, possibly due to the large numerical error from the coarse mesh.

Summary and Outlook

Droplet (fluid) -droplet (fluid) interaction: The collision dynamics of two equal-sized droplets is systematically investigated via three dimensional simulations using a finite volume technique incorporating the volume of fluid (VOF) methodology. Various VOF based models are developed and validated. The ghost cell method is combined with VOF to simulate retarded coalescence collisions. For retarded coalescence collisions, the rupture time of the inter-droplet gas film is predicted by tracking the interface front. An accepted agreement is obtained between simulation and experiment results. The computation suggests that the evolution is relatively insensitive to the resolution of the inter-droplet gas layer. The variation in the inter-droplet pressure depends on the forward velocity of the interface front and the drainage rate of the inter-droplet gas film. A non-dimensionless pressure C_p, defined by the ratio of the inter-droplet pressure to the initial droplet kinetic energy, is introduced to describe the resistance for droplet coalescence. Droplet contact time and maximum non-dimensionless pressure C_p are recommended as criteria for droplet coalescence model. A two-VOF-indicator model is also developed and validated. The combination of VOF model and adaptive mesh refinement technique performs well in enhancing accuracy in the areas of interest and reducing computational cost. In future, droplet coalescence model using droplet contact time and maximum non-dimensionless pressure C_p as criteria will be developed.

Particle (solid) -droplet (fluid) interaction: VOF method coupled with mesh motion in six degrees of freedom (6-DoF) is introduced to model particle-droplet interaction. A brief introduction is given to the CFD model. The advantages of the CFD model are analyzed compared to the conventional energy conservation and force balance approaches. Mesh dependence tests have been performed. The validation of the model with experiment is ongoing. The CFD model has a potential to predict the final results of particle/particulate collisions.

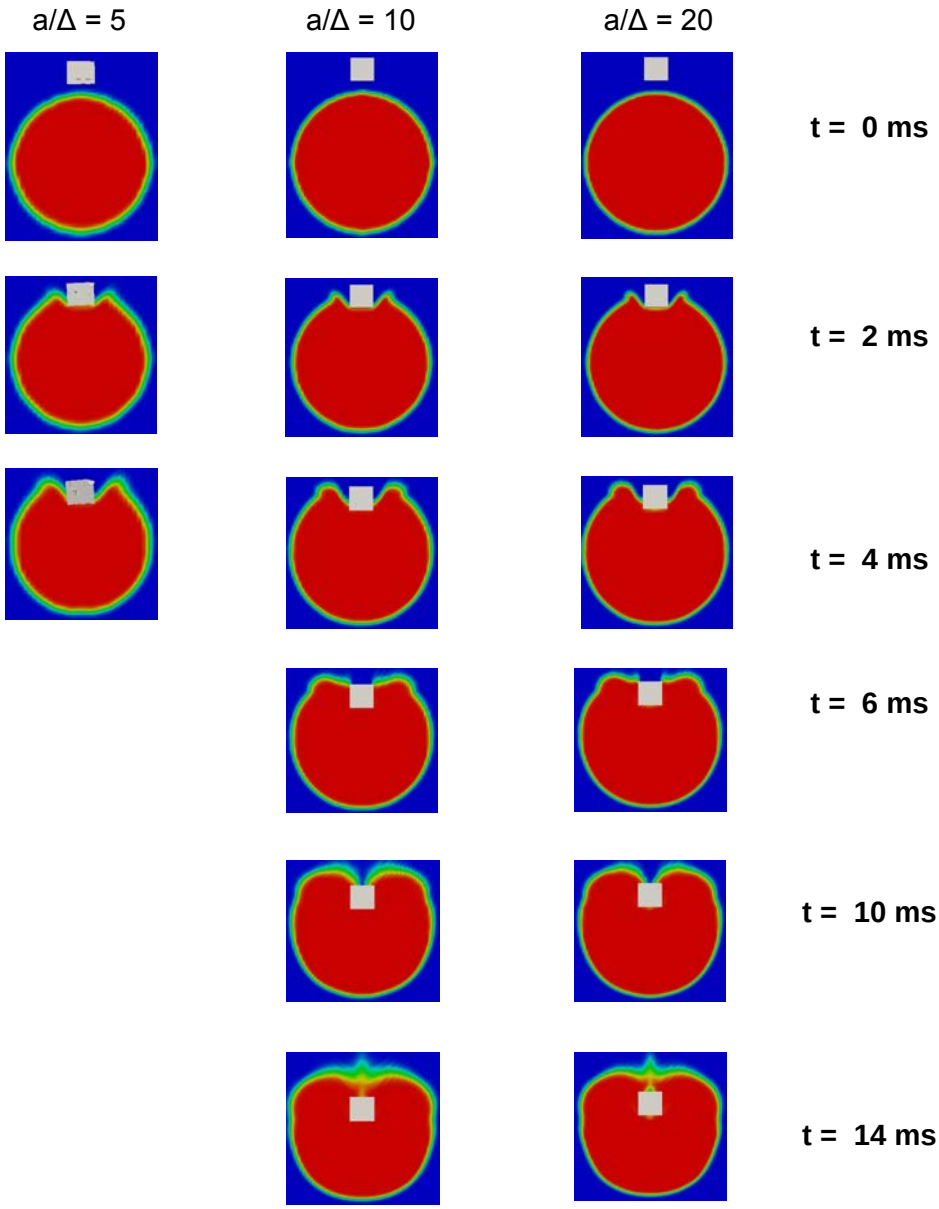

Figure 14: Head-on collision of a cubic particle and a spherical droplet. The size of particle is 10 μm and the relative velocity is 15 m/s. In columns a, b and c, the cubic particle is resolved by 5, 10 and 20 cells, respectively.

References

[1] J. Qian and C.K. Law, Regimes of coalescence and separation in droplet collision, *J. Fluid Mech.*, 1997, 331, 59-80.

[2] http://www.openfoam.com/

[3] X. Jiang and A.J. James, Numerical simulation of the head-on collision of the two equal-sized drops with van der Waals forces, *J. Eng. Math.*, 2007, 59, 99-121.

[4] N. Nikolopoulos, K.S. Nikas and G. Bergeles, A numerical investigation of cenral binary collision of droplets, Computers & Fluids, 2009, 38, 1191-1202.

[5] H. Jasak and A.D. Gosman, Automatic resolution control for the finite volume method, part 2: adaptive mesh refinement and coarsening, Numerical Heat Transfer, Part B, 2000 (38), 257-271.

[6] A. Theodorakakos and G. Bergeles, Simulation of sharp gas-liquid interface using VOF method and adaptive grid local refinement around the interface, Int. J. Numer. Meth. Fluids, 2004, 45, 421-439.

[7] Y. Pan and K. Suga, Numerical simulation of binary liquid droplet collision, Phys. Fluids, 2005, 17, 082105.

[8] http://foam.sourceforge.net/docs/cpp/a08392_source.html

[9] X.G. Li and U. Fritsching, Numerical investigation of binary droplet collisions in all relevant collision regimes, Journal of Computational Multiphase Flows, 2011, 3(4), 207-224.
[10] F. Krause, X. Li and U. Fritsching, Simulation of droplet-formation and -interaction in emulsification process, Engineering Applications of Computational Fluid Mechanics, 2011, 5(3), 406-415.
[11] Y. Wu, J.M. Zhang and E.J. Lavernia, Modeling of the incorporation of ceramic particulates in metallic droplets during spray atomization and co-injection, Metall. Materials Trans. B, 1994, 25, 1, 135-147.
[12] J. Zhang, Y. Wu and E.J. Lavernia, Kinetics of ceramic particulate penetration into spray atomized metallic droplet at variable penetration depth, Acta. Metall. Mater., 1994, 42, 9, 2955-2971.
[13] M. Hoeven, T. Howes, I. Cameron, G. Meesters and H. Wildeboer, Regime map for particle-droplet collisions, Proc. World Cong. Particle Tech. (WCPT 6), 2010.
[14] E. Ekedahl, 6-DOF VOF-solver without damping in OpenFOAM, 2009.
[15] P. Moradnia, A tutorial on how to use dynamic mesh solver icodymfoam, PhD course in CFD with Open-Source software, 2007.